Available online at www.sciencedirect.com

ScienceDirect

Procedia Structural Integrity 42 (2022) 895–902

Structural Integrity Procedia

www.elsevier.com/locate/procedia

23 European Conference on Fracture - ECF23

Impact toughness of an electron-beam welded 0.2C direct-quenched and partitioned steel

Sakari Pallaspuro[a]*, Ann-Christin Hesse[b], Tim Engelke[b], Johannes Sainio[a], Sumit Ghosh[a], Vahid Javaheri[a], Klaus Dilger[b], Jukka Kömi[a]

[a] *Materials and Mechanical Engineering, Centre for Advanced Steels Research, University of Oulu, Finland*
[b] *Institute of Joining and Welding, Technische Universität Braunschweig, Germany*

Abstract

Third generation advanced high-strength steels, e.g., quenched and partitioned steels, are forthcoming structural materials, which consist of a martensitic matrix and a substantial proportion of stabilized residual austenite for improved deformability. A novel less energy-intensive processing route of direct-quenching and partitioning advances this concept by facilitating carbon partitioning to untransformed austenite directly from the quench-stop temperature. However, a major challenge also with these steels is how to maintain structural integrity in the welded end-products after additional heat-input reaching above a temperature where given microstructure is still stable. Heat-input limiting beam welding processes are a solution to this by minimizing degradation of the heat-affected zone (HAZ) and producing even-strength welded joints for S1100 and above. In this study, we report toughness properties of an electron-beam (EB) welded 0.2C-1.5Mn-0.5Si-0.8Al-1.1Cr-0.8Ni (wt.%) direct-quenched and partitioned steel (DQ&P) having a yield strength of ~1100 MPa, and a direct-quenched (DQ) was used as a reference. Low-temperature post-weld heat treatment (PWHT) was considered, too. Weld seam, coarse-grained HAZ, and the base materials were tested for impact toughness. Both the DQ and DQ&P base materials have excellent impact toughness transition temperatures T_{28J} below -100 °C. The weld seam has very good low-temperature toughness already at this stage of optimisation with T_{28J} of -66 °C, which shows robustness of the chosen alloy. Increased residual austenite content increased upper shelf toughness but not T_{28J}. Furthermore, both the DQ and DQP HAZs have T_{28J} below -70 °C, pointing to the weld seam as the weakest link. PWHT reduced low-temperature impact toughness in all the cases with T_{28J} being above -40 °C, clearly demanding reassessment of its feasibility.

* Corresponding author. Tel.: +358 294 487 481.
E-mail address: sakari.pallaspuro@oulu.fi

2452-3216
10.1016/j.prostr.2022.12.113

Keywords: advanced high-strength steel; direct quenching and partitioning; electron-beam welding; post weld heat treatment; impact toughness.

Nomenclature

A	elongation
AHSS	advanced high-strength steel
C_V	Charpy-V impact toughness energy
$C_{V\text{-}min}$	Charpy-V lower shelf energy
$C_{V\text{-}US}$	Charpy-V upper shelf energy
DQ	direct quenching
DQ&P	direct quenching & partitioning
EB	electron beam welding
HAZ	(coarse-grained) heat-affected zone
HV	Vickers hardness
PWHT	post-weld heat treatment
RA	retained austenite
TS	tensile strength
T_{28J}	impact toughness transition temperature
T_{50}	50% upper shelf energy transition temperature
$t_{8/5}$	cooling time from 800 °C to 500 °C (after welding)
WS	weld seam
YS	yield strength

1. Main text

Quenched and partitioned steels, as first proposed by Speer et al. (2003) and Edmonds et al. (2006), are one type of advanced high-strength steels (AHSS), which aim in providing improved deformability via increased residual austenite content. Based on this concept, energy-efficient direct-quenched and partitioned (DQ&P) ultrahigh-strength steels facilitate carbon partitioning to deformed untransformed austenite directly from the quench-stop temperature T_Q (Somani et al. 2018, Kantanen et al. 2019, Ghosh et al. 2022). These 0.2C to 0.4C low-alloy steels have a refined lath-martensitic microstructure with fine film-like inter-lath residual austenite, and with carbon contents up to 0.3C can have extremely good combination of high yield strength ($\gtrsim$ 1100 MPa) and low-temperature impact toughness transition temperature T_{28J} ($\lesssim$ -100 °C) (Somani et al. 2018, Kantanen et al. 2019). With structural applications in mind, their toughness properties in as-welded condition need to be known, too.

Generally, AHSS are prone to softening in the HAZ during welding. Low heat-input beam welding processes are one way to reduce this softening. These processes offer high energy-densities on the surface of the component, leading to vaporization of the material and to a vapor channel in the melt. This vapor channel allows the beam to penetrate deep into the base material, resulting in a deep yet narrow weld seam with a low energy-input per unit length, and short $t_{8/5}$-times. One of the beam welding processes is electron beam welding (EB). In contrast to laser beam welding, EB is conducted in a vacuum chamber, so all interactions of the welding process with the surrounding atmosphere are inhibited. Furthermore, modern EB machines allow quick manipulation of the position of the electron beam. This leads to the possibility to weld structures at multiple spots at the same time without a collapse of the keyhole. These machines are also capable of changing the beam pattern in certain ways. Through this, the shape of the molten area, melt pool dynamics, and the keyhole behaviour can be influenced. One practical use of this possibility is the adjustment of the fusion line so that it is perpendicular to the surface of the base material. This is beneficial for Charpy impact tests or fracture mechanics tests if certain areas in the HAZ (e.g., the coarse-grain HAZ) need to be tested. Few studies have so far considered these aspects in quenched and partitioned steels (Forouzan et al. 2017, Zurnadzhy 2019, Zhang et al. 2021).

2. Materials & Methods

2.1. Materials

The studied material is a vacuum-cast low-alloy steel with a chemical composition of 0.22C – 1.50Mn – 0.53Si – 0.83Al – 1.10Cr – 0.75Ni and with P/S/O/N ≤ 0.002 (wt.%). This results in carbon equivalents CE_{IIW} = 0.74 and CET = 0.44 (EN 1011-2 2001), i.e., the alloy should have poor weldability, be susceptible to cold cracking, and need pre-heating for both matters. The steel plates were made by first annealing blocks (L 110 x W 80 x H 60 mm) cut from the cast for 2 hours at 1200 °C, and then laboratory hot-rolling them in two stages, both with 4 passes and ~0.2 strain/pass, at temperatures both above and below the non-recrystallisation temperature: first stage prior-austenite grain refining rolling was done to a 26 mm thickness with the last pass at ~1030 °C, and the second stage prior-austenite grain deforming rolling to a final thickness of 11 mm with the final pass at ~820 °C. Direct-quenched and partitioned plates (DQ&P) were immediately quenched in water to a quench-stop temperature T_Q of ~275 °C, and subjected to partitioning in a furnace pre-heated to the same temperature, and the off-switched furnace was let to cool down, simulating slow cooling of an industrial strip coil. The reference direct-quenched plates (DQ) were cooled in water directly to ambient temperature. The resulting microstructure of the DQ&P steel is fine-scale lath-martensitic with a pronounced fraction of film-like residual austenite and some carbides precipitated during the partitioning, and DQ is essentially as-quenched lath-martensitic (DQ). Table 1 shows the mechanical properties of these materials, as reported for the same alloy and near-identical processing by Somani et al. (2018).

Table 1. Mechanical properties of the base materials, according to Somani et al. (2018). YS = yield strength, TS = tensile strength, A = total elongation, A_g = uniform elongation, HV = Vickers hardness, RA = residual austenite vol.%, and DL = detection limit.

Material	YS [MPa]	TS [MPa]	A [%]	A_g [%]	HV	RA [%]
DQ	1360	1690	12	3	505	< DL
DQ&P	1130	1560	12	4	470	7

2.2. Welding

Electron-beam welding was carried out in a pro-beam K26-3 welding chamber. The specimens were grinded and cleaned on the top and bottom surfaces to reduce possible inclusions during welding. Before welding, they were also demagnetized to avoid any deflection of the electron beam.

For welding, a voltage of 120 kV, a beam current of 37 mA, and a welding speed of 10 mm/s were used. The focus was on the top surface of the specimen with a focal distance of 626 mm. In order to produce weld seams with a width that is representable for practical applications and a straight fusion line, beam oscillation with a figure 8 pattern was used. The pattern had an amplitude of 1.3 mm in welding direction and transverse to welding direction, and was repeated with a frequency of 600 Hz. A weld backing made from steel with a similar chemical composition was used to prevent sagging of the liquid metal during welding. Welding was carried out transverse to rolling direction.

Thermocouples were used to measure temperatures in the HAZ to determine pre- and post-heating temperatures as well as the cooling time $t_{8/5}$. The thermocouples showed that the upper surface of the specimens heated up to around 30 °C to 45 °C before welding due to the positioning of the specimens with the X-ray image, see number 1 in the graph in Fig. 1. The welding resulted in $t_{8/5}$-times of 2.20 s to 2.26 s. Compared to arc-welding processes, these $t_{8/5}$-times are rather short.

In order to consider the effect of post-weld heat treatment, a heat treatment with a peak temperature of 275 °C was chosen for some of the welded plates. A direct stop of the cooling after welding at 275 °C was not possible as the specimens could not be heated during the flooding of the vacuum chamber. After flooding, the specimens had a temperature of around 90 °C in the HAZ, see number 2 in the graph in Fig. 1 b. They were transferred to a furnace and heated to T_Q = 275 °C. After holding the specimens at this temperature for one hour, they were cooled in air down to room temperature.

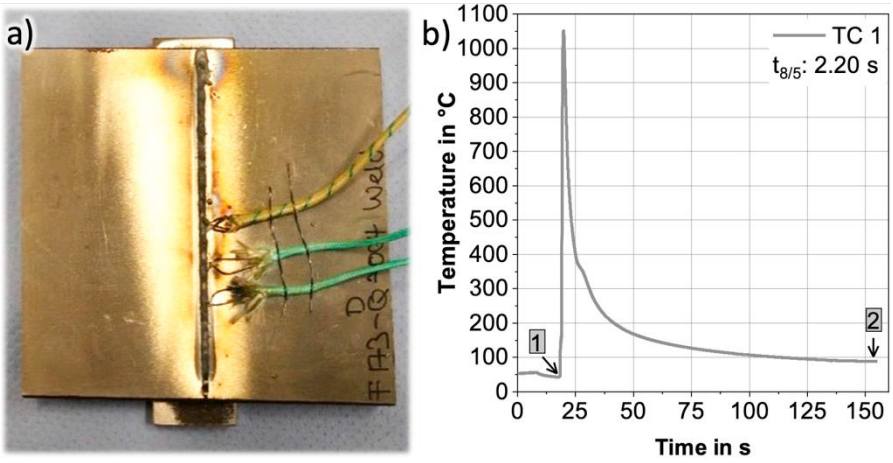

Fig. 1. a) Welding setup with thermocouples, and b) temperature history next to fusion line.

2.3. Mechanical testing

For every series, a cross section in the middle of the weld seam was taken. Hardness indentations with HV_1 and 250 µm spacing were done on five lines across the weld seam. The lines were taken at 1 mm distance from the top and bottom surface of the specimens as well at 1/3, 1/2 and 2/3 of the sheet thickness.

Charpy impact toughness testing was done on 9 mm thick Charpy-V specimens according to EN ISO 148-1 (2016) with a notch in the thickness direction of the sheets. The orientation of the specimens was parallel to the rolling direction of the base material. Testing was done at temperatures between room temperature and -196 °C. For the welded specimens, two different notch positions were considered: One was the coarse-grain heat affected zone (HAZ) in direct proximity to the fusion line, and one was in the middle of the weld seam itself. After testing, all specimens were checked for possible fracture path deviation. Evaluation of the data was done according to the procedure proposed by Wallin (2011), which uses a tanh-function of Eq. (1):

$$C_V = \frac{C_{V-US}-C_{Vmin}}{2} \times \left(1 + tanh\left(\frac{T-T_{50}}{C}\right)\right) + C_{Vmin} \quad (1)$$

3. Results and Discussion

The EB welded cross-sections are presented in Fig. 2 and the measured hardness values for the materials in Table 2. Most importantly, the chosen welding parameters and $t_{8/5} \approx 2.2$ result in even hardness between the weld seam (WS) and DQ&P base material, while DQ has near 500 HV_1 base material hardness. Although it cannot prove equal mechanical properties, achieved same hardness indicates low mismatch between DQ&P and WS. Both base material hardnesses are on the same level as with Somani (2018), which justifies assuming mechanical properties given in Table 1. Softest part in HAZ locates within 0.5 mm from the fusion line, and is ~120 HV_1 softer than the weld seam. PWHT softens the microstructures by 20 HV_1 on average. Surprisingly, also DQ&P base material softens to a degree with PWHT, implying that the microstructure has not been fully stabilised at given T_Q.

Table 2. Hardness of the base materials and weldments
(WS = weld seam, HAZ = heat-affected zone hardness minima, PWHT = post-weld heat treatment).

	DQ	DQ&P	EB WS	EB HAZ	DQ PWHT	DQ&P PWHT	EB WS PWHT	EB HAZ PWHT
HV_1 (avg. ± S.D.)	494 ± 5	455 ± 5	461 ± 9	338 ± 14	472 ± 5	437 ± 10	443 ± 9	343 ± 15

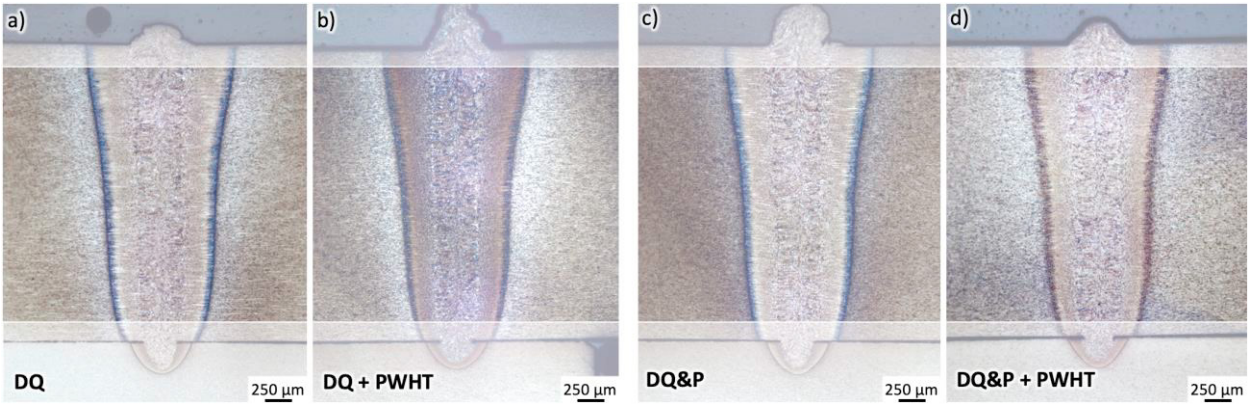

Fig. 2. The as-welded cross sections for: a) DQ, b) DQ + PWHT, c) DQ&P, and d) DQ&P + PWHT (PWHT = post-weld heat treatment).

The Charpy-V impact toughness results are summarised in Table 3, and the fitted ductile-brittle transition curves in Figs. 3 and 4. DQ&P has clearly higher fitted upper shelf energy $C_{V\text{-}US}$ (+ 49 %) when compared to the essentially martensitic DQ. None of the cases have particularly poor upper shelf energy as the lowest average value of 91 J is with the weld seam. With lowering temperature, DQ&P has still marginally higher impact toughness over DQ at -40 °C. As tested with samples at -196 °C (outside the plots of Figs. 3 and 4), both DQ&P base material and the weld seam have a minimum impact toughness of 5 ± 0.3 J (7 J/cm^2), which is further used as $C_{V\text{-}min}$ in all the fittings (Eq. 1). This also shows that the increased residual austenite does not contribute to energy absorption at low temperatures in a significant manner.

The base materials have excellent impact toughness transition temperature T_{28J} levels below -100 °C (Fig. 3 a-b), especially when considering the yield strength >1300 MPa for DQ and >1100 MPa for DQ&P. The base material results, both upper shelf energies and T_{28J}, are in line with what reported by Somani et al. (2018) with the same alloy and near-identical processing. Small variations can be explained by natural scatter in impact toughness and significantly higher test numbers in the present study. The weakest link, the weld seam, has still very good T_{28J} at below -60 °C (Fig. 3 c), too.

HAZ / fusion line notch position results in upper shelf values and T_{28J} temperatures between the base materials and the weld seam. These HAZ specimens are also prone to crack path deviation in the upper shelf regime, which is seen as increased scatter (Fig. 4). Generally, the results indicate that with well-controlled beam welding process these ultrahigh-strength steels could well be considered for structural applications exposed to low temperatures.

Table 3. Summarised average upper shelf energies ($C_{V\text{-}US}$) and impact toughness at -40 °C ($C_{V\text{-}40°C}$), and the characteristic ductile-brittle transition temperatures.

	$C_{V\text{-}US}$ [J/cm^2]	$C_{V\text{-}40°C}$ [J/cm^2]	T_{50} [°C]	T_{35J/cm^2} [°C]	T_{28J} [°C]
DQ (BM)	84	68 ± 4	-88	-107	-104
DQ&P (BM)	125	75 ± 7	-55	-105	-103
EB WS	91	39 ± 7	-39	-69	-66
EB WS + PWHT	94	25	-18	-36	-33
DQ HAZ	94	51 ± 10	-52	-88	-86
DQ HAZ + PWHT	120	54 ± 16	-3	-42	-39
DQ&P HAZ	117	39 ± 7	-31	-81	-78
DQ&P HAZ + PWHT	99	32	-24	-42	-39

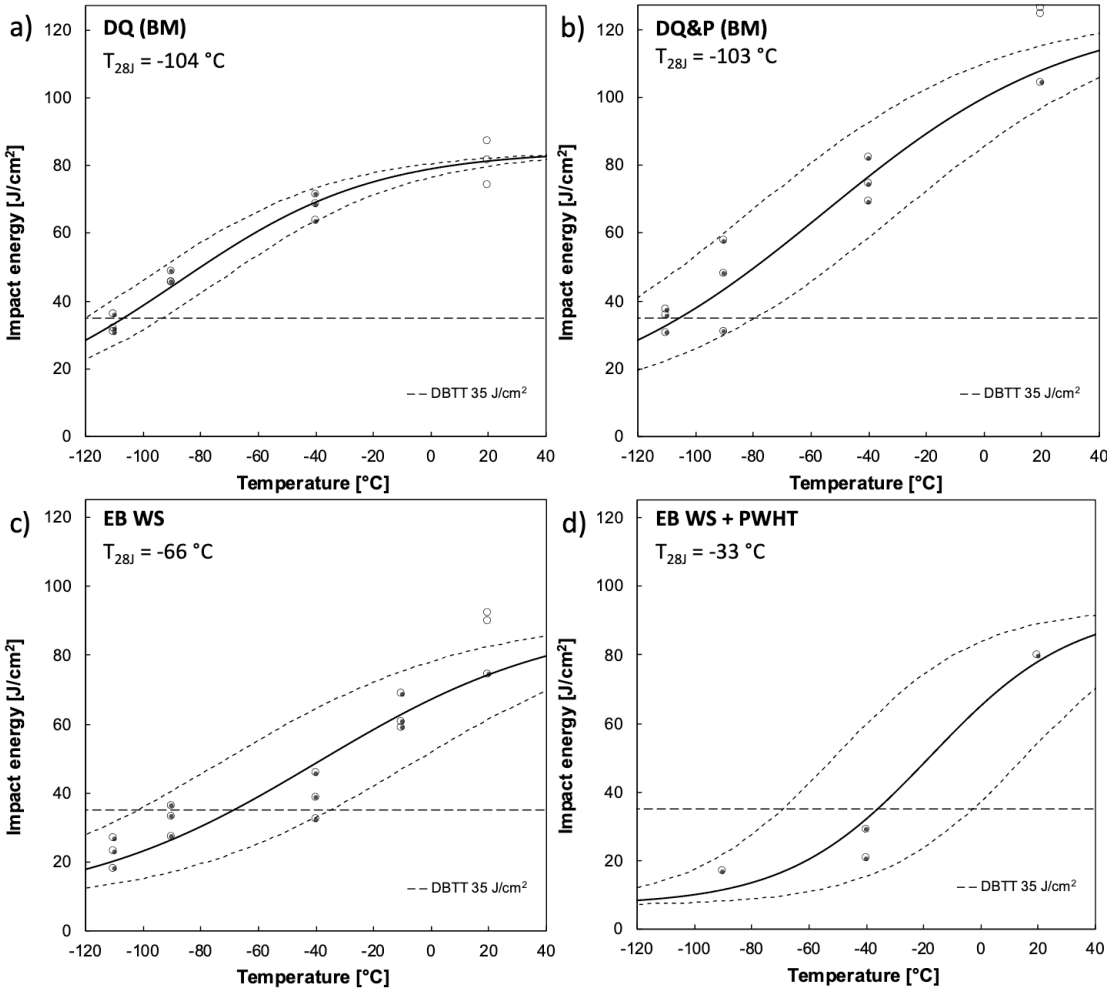

Fig. 3. Impact toughness results for: a) DQ base material (BM), b) DQ&P base material, c) electron-beam welded weld seam (EB WS), and d) post-weld heat-treated WS.

Post-weld heat treatment conducted at T_Q = 275 °C reduces low-temperature toughness properties in all the cases, and for HAZ cases the changes are within scatter due to crack path deviation (Fig. 4). With PWHT, T_{28J} raises 33 °C to -33 °C for EB WS + PWHT, 47 °C to -39 °C for DQ HAZ + PWHT, and 39 °C to -39 °C for DQ&P HAZ + PWHT. Unfortunately, direct observations of why this happens are missing from this study. However, the results are in line with Pallaspuro (2018) showing impairment in toughness properties with low-temperature tempering for initially tough as-quenched ultrahigh-strength steels due to carbide enrichment and consecutive rise in yield strength.

The benefits of finely distributed film-like residual austenite, which is more stable than blocky type (Gao et al. 2014), have been reported also elsewhere for quenched and partitioned steels (Gao et al. 2014, Somani et al. 2018, An et al. 2019, Kantanen et al. 2019, Yang et al. 2021). Furthermore, larger blocky C-rich retained austenite islands act as very acute failure initiation sites when transformed to martensite under straining (Gao et al. 2014), and are therefore unwanted. Lower carbon contents up to 0.3 C wt.% appear to provide good toughness (Kantanen et al. 2019, Yang et al. 2021), but 0.4 C wt.% steels are already divisive: impact toughness can be good with lower TS (Gao et al. 2014, An et al. 2019), but with microstructures hardening above 2000 MPa, the resulting impact toughness is still unavoidably lower (Zurnadzhy et al. 2019, Ghosh et al. 2022). In these low-alloyed carbon-steels, moderate retained austenite fractions $\lesssim$ 10 vol.% appear to provide the best toughness when associated with film-like morphology, as shown in this study and by Somani et al. (2018) and Kantanen et al. (2019), while higher RA fraction could introduce blocky islands.

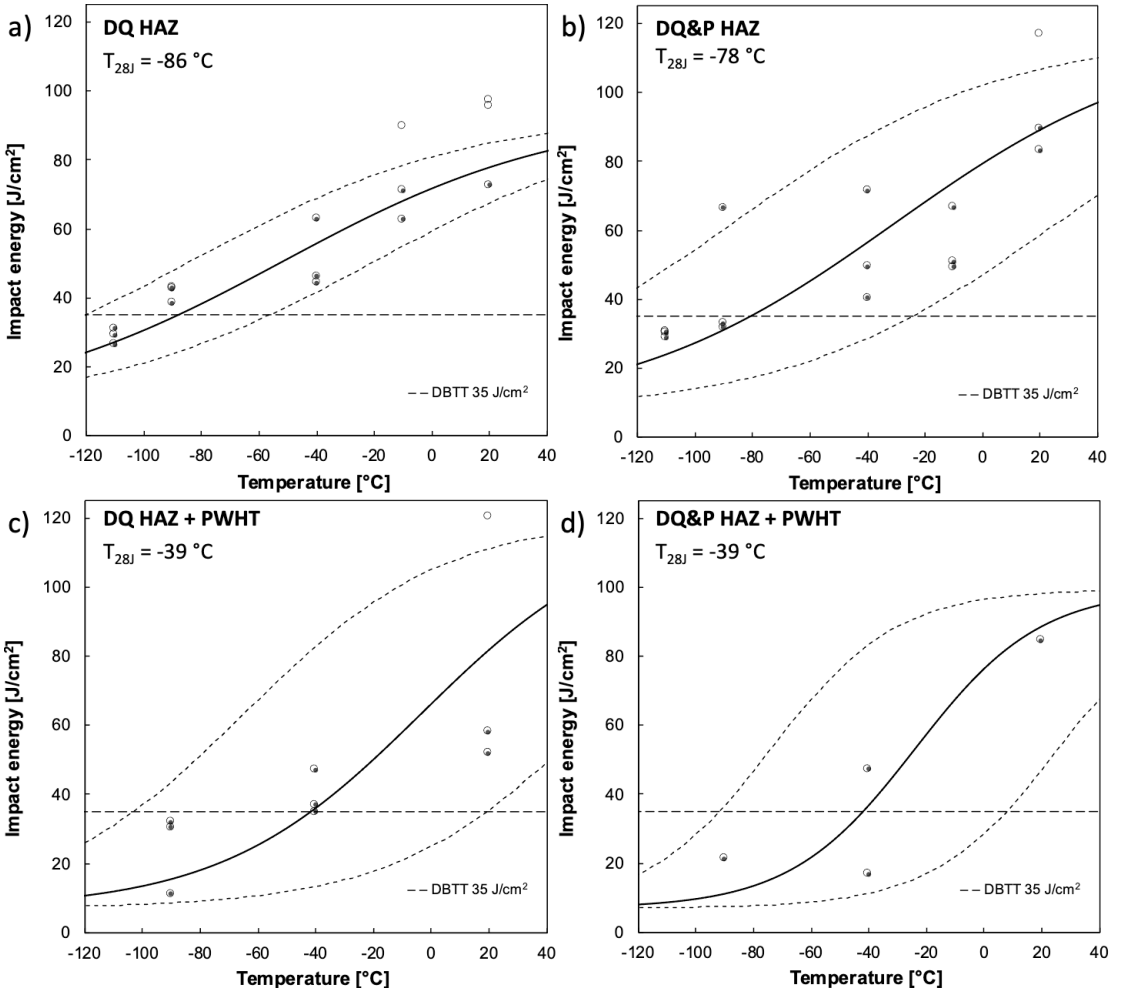

Fig. 4. Impact toughness results for the coarse-grain heat-affected zone / fusion line notch position: a) DQ HAZ), b) DQ&P HAZ, c) electron-beam welded weld seam (EB WS), and d) post-weld heat-treated WS.

Compared to the literature, the steels and welds presented here perform well: performance of DQ&P is on par with 0.2C DQ&P variants reported by Somani et al. (2018) and 0.3C DQ&P steels reported by Kantanen et al. (2018). To the best knowledge of the authors, these direct-quenched and partitioned ultrahigh-strength steels have the best low-temperature toughness properties within 3rd generation advanced high-strength steels. Furthermore, the weld seam has the highest reported low-temperature impact toughness for quenched and partitioned steels in as-welded condition, having superior T_{28J} over most of the base materials reported in the literature. Could these toughness properties be improved further? A possible solution would be utilising higher quench-stop / partitioning temperatures, which would both make the microstructures stable at higher temperatures, therefore suppressing HAZ, and likely improve deformability via increased residual austenite content (Somani 2018), if blocky RA can be avoided. Further work will continue on fracture mechanical properties of the same materials presented in this study.

4. Conclusions

A martensitic-austenitic direct-quenched and partitioned (DQ&P) 0.2C steel and a direct-quenched reference (DQ) from the same alloy were electron-beam welded and studied for impact toughness properties to evaluate weldability and low-temperature toughness properties of the base materials, weld seam, and heat-affected zone. The main findings are:

- Electron-beam welding produces martensitic welds with near-straight fusion lines, and with $t_{8/5} \approx 2.2$ s a weld-seam hardness of ~460 HV1, which is within standard deviation of that of DQ&P, indicating low mismatch on mechanical properties.

- Both the DQ&P and DQ base materials have excellent impact toughness transition temperature T_{28J} below -100 °C. More importantly, also the electron beam welded weld seam has T_{28J} of -66 °C without post-processing of the welds. Impact toughness for the notches positioned at coarse-grained heat-affected zone have T_{28J} between the base materials and the weld seam, but these samples were also prone to crack path deviation. Thus, weld seam is the weakest link in the sampled cases.

- Post-weld heat treatment (PWHT) conducted at the partitioning start temperature of 275 ºC reduced impact toughness in all the cases throughout the ductile-brittle transition regime. This is in line with other studies showing impairment in toughness properties with low-temperature tempering for initially tough as-quenched ultrahigh-strength steels. All the PWHT treated cases had $T_{28J} < -30$ °C, which is still fair for welded microstructures with expected yield strength well above 1000 MPa. These results highlight a clear demand for reassessment of need for PWHT.

Acknowledgements

The authors wish to thank Business Finland for funding this research through the FOSSA program. The technical help of Jussi Paavola, Tun Tun Nyo, and Ilpo Alasaarela is thanked, too. In addition, the role of Nora in the finalisation of this study is greatly appreciated.

References

An, B., Zhang, C., Gao, G., Gui, X., Tan, Z., Misra, R.D.K., Yang, Z., 2019. Experimental and theoretical analysis of multiphase microstructure in a newly designed MnSiCrC quenched and partitioned steel to promote bainitic transformation: The significant impact on mechanical properties. Materials Science and Engineering: A 757, 117-123.

Edmonds, D.V., He, K., Rizzo, F.C., De Cooman, B.C., Matlock, D.K., Speer, J.G., 2006. Quenching and partitioning martensite—A novel steel heat treatment. Materials Science and Engineering: A 438-440, 25-34.

EN ISO 148-1:2016. Metallic Materials – Charpy pendulum impact test – Part 1: Test method. 29.

Forouzan, F., Vuorinen, E., Mücklich, F., 2017. Post weld-treatment of laser welded AHSS by application of quenching and partitioning technique. Materials Science and Engineering: A 698, 174-182.

Gao, G., Zhang, H., Gui, X., Luo, P., Tan, Z., Bai, B., 2014. Enhanced ductility and toughness in an ultrahigh-strength Mn–Si–Cr–C steel: The great potential of ultrafine filmy retained austenite. Acta Materialia 76, 425-433.

Ghosh, S., Kaikkonen, P., Javaheri, V., Kaijalainen, A., Miettunen, I., Somani, M., Kömi, J., Pallaspuro, S., 2022. Design of tough, ductile direct quenched and partitioned advanced high-strength steel with tailored silicon content. Journal of Materials Research and Technology 17, 1390-1407.

Kantanen, P., Somani, M., Kaijalainen, A., Haiko, O., Porter, D., Kömi, J., 2019. Microstructural Characterization and Mechanical Properties of Direct Quenched and Partitioned High-Aluminum and High-Silicon Steels. Metals 9, 256.

Pallaspuro, S., 2018. On the factors affecting the ductile-brittle transition in as-quenched fully and partially martensitic low-carbon steels. Acta Universitatis Ouluensis C 655.

Somani, M., Porter, D., Kömi, J., Karjalainen, L.P., Misra, D.K., 2018. Tough Ductile Ultra High Strength Steels Through Direct Quenching and Partitioning – An Update. Proceedings of the International Conference on Martensitic Transformations: Chicago, 139-134.

Speer, J., Matlock, D.K., De Cooman, B.C., Schroth, J.G., 2003. Carbon partitioning into austenite after martensite transformation. Acta Materialia 51, 2611-2622.

Wallin, K., 2011. Fracture Toughness of Engineering Materials – Estimation and Application. EMAS Publishing, Warringon, 566.

Yang, K., Li, Y., Hong, Z., Du, S., Ma, T., Liu, S., Jin, X., 2021. The dominating role of austenite stability and martensite transformation mechanism on the toughness and ductile-to-brittle-transition temperature of a quenched and partitioned steel. Materials Science and Engineering: A 820, 141517.

Zhang, W., Tao, W., Yang, S., 2021. Mechanical properties and fracture behaviors in remote laser spot welding of quenching and partitioning 980 steel. Optics & Laser Technology 140, 107053.

Zurnadzhy, V.I., Efremenko, V.G., Wu, K.M., Azarkhov, A.Y., Chabak, Y.G., Greshta, V.L., Isayev, O.B., Pomazkov, M.V., 2019. Effects of stress relief tempering on microstructure and tensile/impact behavior of quenched and partitioned commercial spring steel. Materials Science and Engineering: A 745, 307-318.